Check for updates

Tribbles Homolog 3 Mediates the Development and Progression of Diabetic Retinopathy

Priyamvada M. Pitale,[1] Irina V. Saltykova,[1] Yvonne Adu-Agyeiwaah,[2] Sergio Li Calzi,[2] Takashi Satoh,[3] Shizuo Akira,[4] Oleg Gorbatyuk,[1] Michael E. Boulton,[2] Machelle T. Pardue,[5] W. Timothy Garvey,[6] Mohammad Athar,[7] Maria B. Grant,[2] and Marina S. Gorbatyuk[1]

Diabetes 2021;70:1738–1753 | https://doi.org/10.2337/db20-1268

The current understanding of the molecular pathogenesis of diabetic retinopathy does not provide a mechanistic link between early molecular changes and the subsequent progression of the disease. In this study, we found that human diabetic retinas overexpressed TRIB3 and investigated the role of TRIB3 in diabetic retinal pathobiology in mice. We discovered that TRIB3 controlled major molecular events in early diabetic retinas via HIF1α-mediated regulation of retinal glucose flux, reprogramming cellular metabolism, and governing of inflammatory gene expression. These early molecular events further defined the development of neurovascular deficit observed in mice with diabetic retinopathy. TRIB3 ablation in the streptozotocin-induced mouse model led to significant retinal ganglion cell survival and functional restoration accompanied by a dramatic reduction in pericyte loss and acellular capillary formation. Under hypoxic conditions, TRIB3 contributed to advanced proliferative stages by significant upregulation of GFAP and VEGF expression, thus controlling gliosis and aberrant vascularization in oxygen-induced retinopathy mouse retinas. Overall, our data reveal that TRIB3 is a master regulator of diabetic retinal pathophysiology that may accelerate the onset and progression of diabetic retinopathy to proliferative stages in humans and present TRIB3 as a potentially novel therapeutic target for diabetic retinopathy.

PATHOPHYSIOLOGY

The pathological retinal lesions of diabetic retinopathy (DR) in humans include an early asymptomatic phase, nonproliferative phase (NPDR), and late phase known as proliferative DR (PDR). Treatments of severe NPDR with intraretinal hemorrhages and PDR are often focused on vascular abnormalities presented as microaneurysm, vascular leakage, capillary blockade and dropouts, acellular capillaries, and aberrant angiogenesis. Mild and moderate forms of NPDR in patients are controlled by monitoring blood glucose level (BGL) and blood pressure. Although clinical evidence clearly demonstrates that the management of BGL implemented early in the course of diabetes may reduce the development and progression of NPDR (1), a breakthrough treatment that interferes with early DR stages, thus preserving retinal integrity against subsequent damage and preventing progression of DR, remains an unmet critical need.

The tribbles homolog 3 (TRIB3) protein has been proposed as a regulator of insulin signaling in diabetes. TRIB3 is a metabolic stress indicator and is a critical "stress-adjusting switcher," endorsing cell homeostasis shift to metabolic dysfunction. It functions by regulating AKT and AKT/mTOR phosphorylation through pseudokinase activity and controlling autophagy flux and protein degradation (2). TRIB3 overexpression has been linked to aberrant angiogenesis. In a study that used human

[1]Department of Optometry and Vision Science, School of Optometry, University of Alabama at Birmingham, Birmingham, AL
[2]Department of Ophthalmology and Visual Sciences, University of Alabama at Birmingham, Birmingham, AL
[3]Department of Immune Regulation, Tokyo Medical and Dental University, Tokyo, Japan
[4]WPI Immunology Frontier Research Center, Osaka University, Osaka, Japan
[5]Department of Biomedical Engineering, Georgia Institute of Technology, and Atlanta VA Center of Excellence for Visual and Neurocognitive Rehabilitation, Atlanta, GA
[6]Department of Nutrition Sciences and Department of Dermatology, University of Alabama at Birmingham, Birmingham, AL
[7]School of Medicine, University of Alabama at Birmingham, Birmingham, AL
Corresponding author: Marina S. Gorbatyuk, mgortk@uab.edu

Received 18 December 2020 and accepted 4 May 2021

This article contains supplementary material online at https://doi.org/10.2337/figshare.14541915.

© 2021 by the American Diabetes Association. Readers may use this article as long as the work is properly cited, the use is educational and not for profit, and the work is not altered. More information is available at https://www.diabetesjournals.org/content/license.

umbilical vein endothelial cells treated with oxidized phospholipids, the induction of vascular endothelial growth factor (VEGF) strongly correlated with the highest level of TRIB3 (3). Mechanistically, TRIB3 reportedly regulates the nuclear factor-κB (NF-κB) pathway (4), promotes activation of transforming growth factor-β1 signaling (5), controls cytokine expression (6), and governs macrophage health (7).

Recent studies conducted in patients with type 2 diabetes revealed that the expression of single nucleotide polymorphism Q84R in TRIB3 can increase the risk of diabetes and the likelihood of carotid atherosclerosis in part through the effects of abdominal obesity, hypertriglyceridemia, and insulin resistance in the body (8). These studies have also emphasized that the variant with arginine at position 84 manifests a gain-of-function effect due to TRIB3's superior pseudokinase activity in binding AKT and inhibiting insulin-stimulated AKT phosphorylation (Thr308, Ser473) (9–11). *TRIB3* mRNA and protein are significantly elevated in human type 2 diabetes islets, and a substantial reduction of C-peptide has been observed in the plasma of Q84R allele carriers (12). Q84R polymorphism frequently manifests not only as aberrant insulin signaling but also with vascular dysfunction and metabolic abnormalities (13). All of these events occur in the diabetic retina as well.

Furthermore, clinical research conducted with human fibrovascular membranes excised from patients with PDR showed elevated levels of TRIB3 (14). However, the exact mechanistic link between TRIB3 overexpression and disease development and progression in DR has not been established. In this study, we explored the effects of abrogated TRIB3 expression in the survival of retinal ganglion cells (RGCs), endothelial cells, and pericytes in diabetic mice. Our data reveal a distinct underlying mechanism that involves reduced hypoxia-regulated GLUT1 and EGFR signaling, which contributes to diminishing neovascularization (NV) in DR. Using mouse models of pharmacologically induced diabetes and hypoxia-driven proliferative retinopathies, we demonstrate for the first time that TRIB3 is a potentially novel therapeutic target that may accelerate the onset and progression of DR to proliferative stages in humans.

RESEARCH DESIGN AND METHODS

Detailed information is provided in Supplementary Table 1.

Animals

Mice were housed in a 12-h light-dark cycle condition with unlimited access to food and water at a University of Alabama (UAB) animal facility according to institutional animal care and use committee UAB-IACUC protocol no. 09793 and the Association for Research in Vision and Ophthalmology guidelines on the use of animals in ophthalmic and vision research. TRIB3 knockout (KO) mice generated as previously described (15) were crossed with C57BL/6J mice at least eight times. C57BL/6J mice were purchased from The Jackson laboratory. We intraperitoneally injected 8-week-old males with either five consecutive doses of 50 mg/kg streptozotocin (STZ) to induce diabetes or vehicle (0.1 mol/L citrate buffer, pH 4.5) and assessed 32 weeks later. To observe early metabolic and proinflammation retinal changes, we used a proposed mouse model with a single injection of 150 mg/kg STZ or vehicle and performed the analysis at 4 or 6 weeks postinjection. Blood was collected via a tail vein, and fasting BGLs and HbA_{1c} were measured using a glucometer and HbA_{1c} kit, respectively (Supplementary Table 2). Hyperglycemia was confirmed as fasting BGL >250 mg/dL and >6.5% HbA_{1c}. The animals did not require insulin injections. We also measured retinal glucose levels (RGLs) using a calorimetric assay kit. To mimic proliferative retinopathy, we used a previously described mouse model of oxygen-induced retinopathy (OIR), exposing mice to 75% oxygen levels from postnatal day 7 (P7) and placing them in room air with 21% oxygen at P12 (16). TRIB3 KO and C57BL/6J pups demonstrated no differences in weight gain during normal development. Additionally, we observed no differences among strains after exposing the pups to oxygen.

Quantitative Real-time PCR and Western Blot Analysis

Four weeks post–STZ injection, mouse retinas were isolated, and RNA was extracted using TRIzol. cDNA was synthesized using the iScript Reverse Transcription Supermix Kit (Bio-Rad Laboratories). A QuantStudio 3 machine (Thermo Fisher Scientific) was used to perform quantitative real-time PCR using TaqMan primers (Thermo Fisher Scientific) (Supplementary Table 1). Results were normalized to housekeeping genes *Gusb* and *Gapdh* and expressed as ratios of mRNA fold changes obtained in diabetic retinas normalized to own nondiabetic controls. For protein analysis, retinal protein extracts were isolated from the OIR and control pups at P13 and separated by PAGE. Detection of proteins was performed using anti-VEGF, antiglia fibrillary acidic protein (GFAP), and anti–b-actin antibodies detecting 21-, 50-, and 42-kDa bands, respectively. Horseradish peroxidase (HRP) goat anti-mouse and infrared goat anti-mouse antibodies were used as secondary antibodies (Supplementary Table 1). Immunoblots were imaged and analyzed using the LI-COR imager system. Differences in VEGF and GFAP levels in diabetic retinas are presented as ratios of band intensities normalized to nondiabetic controls.

Histological and Immunohistochemical Analyses

Human retinas from five patients with diabetes and five control individuals were subjected to immunohistochemical (IHC) analysis with anti-TRIB3 antibody. The group with diabetes included the retinas of 62-, 62-, 82-, 84-, and 92-year-old patients, while the control group included the retinas of 66-, 77-, 77-, 78-, and 82-year-old individuals.

Retinal tissues were obtained from the National Disease Research Interchange. In addition, the representative tissues were processed for IHC analysis using anti-CD31 antibody. Before the IHC procedure, sections were deparaffinized and rehydrated by immersing the slides in xylene and alcohol of descending concentrations.

Diabetic and OIR mice were subjected to enucleation at 32 weeks post–STZ injection and at P17, respectively. The eyes were fixed for 3.5 h in 4% paraformaldehyde and stored in 30% sucrose before cryopreservation in optimal cutting temperature (OCT) compound. Retinal sections (12 μm) were stained with hematoxylin-eosin. An investigator blinded to the results counted the number of RGCs and the thicknesses of the inner nuclear layer (INL), outer plexiform layer (OPL), and inner plexiform layer (IPL). For evaluation of the pericyte loss and formation of acellular capillaries, fixed eyes were washed in 1× PBS, and the retina cups were excised. After digestion, separated retinal vascular tissues were placed on a slide, dried out at room air temperature, and stained with periodic acid Schiff reagent. IHC analysis was performed on retinal sections using anti-TRIB3, anti-GFAP, BRN3A, CD31/PECAM-1, and vimentin antibodies (Supplementary Table 1). Colocalization of individual TRIB3 and CD31/PECAM-1, TRIB3 and BRN3A, or GFAP and vimentin proteins in the retinal sections were detected using fluorescent confocal microscopy. Florescence intensity was measured using ImageJ software. Absorption control was performed using the recombinant human TRIB3 protein. To count ionized calcium-binding adaptor molecule 1 (IBA1)–positive microglial cells at P30, mice were injected intraperitoneally with 10 μL/g (stock solution of 1 mg/mL) of lipopolysaccharide (LPS). The eyes were enucleated 24 h after the injection, cryosectioned, and subjected to immunostaining with anti-IBA1 antibody. Investigators blinded to the results counted the number of IBA1 positive cells in the retinal sections.

For detection of NV, the eyes of the OIR pups were enucleated at P17, fixed for 1.5 h, and incubated with isolectin 1B-4 diluted in 1× PBS overnight. After washing with PBS + 0.02% Triton, the retinal cups were dissected to obtain flat mounts. The flat mount images were used to run a computer program developed by Xiao et al. (17) to analyze areas of NV and vaso-obliteration (VO). The retinal NV and VO were expressed as ratios of the area with NV or VO to the whole mouse retina.

Retinal Physiology

At 32 weeks post–STZ injection, the mice were anesthetized to perform electroretinography using a UTAS BigShot LKC machine to measure RGC function. Mice were exposed to 15 sweeps (1 s apart) of white flash of 2.5 candela/m^2 with a white background of 25 candela/m^2 intensity to measure the photopic negative response (PhNR) amplitude. The waveforms were measured using LKC EM software.

Seahorse Measurement

In Seahorse analysis, the extracellular acidification rate (ECAR) and oxygen consumption rate (OCR) were measured at baseline and post–glucose injection and post–oligomycin injection. The eyes were collected 4 weeks post–STZ injection in cold 1× PBS. The retinal cup without retinal pigment epithelium was dissected in Seahorse XF DMEM containing 5 mmol/L HEPES and 2 mmol/L glutamine with no glucose. Retinas were placed with RGC layer facing down (Supplementary Fig. 1) and secured by the capture screen using an insert tool in each well of a Seahorse XF24 Islet Capture microplate containing 50 μL of Seahorse XF DMEM. After securing retinas in the microplate, 400 μL of the same dissecting medium were added to each well for a final volume of 450 μL. The microplate was placed in the incubator at 37°C for a 1-h non-CO_2 incubation before starting the stress test assay to achieve an even CO_2 distribution. The ports of the Seahorse XF24 Sensor Cartridge were loaded for a final well concentration of 10 mmol/L glucose and 3.0 μmol/L oligomycin for measuring pH and O_2. Seahorse Wave Desktop Software was used to analyze the data.

Cell Culture Experiments

MIO-M1 cells (immortalized human Müller glia cell line developed by Limb et al. in 2002 [18]) were cultured at 37°C in Dulbecco's modified Eagle's medium supplemented with high glucose (25 mmol/L glucose), 10% FBS and 1% antibiotic solution. Cells were exposed to hypoxia or treated with advanced glycosylation end products (AGE) and BSA at a dose of 500 mmol/L for 48–72 h. Protein was extracted using radioimmunoprecipitation lysis buffer. Western blot analysis was performed using the anti-TRIB3 antibody and HRP-conjugated goat anti-mouse secondary antibody.

Experiments were also performed with MIO-M1 cells overexpressing mouse TRIB3-DDK for 72 h. The cells were harvested, lysed in the immunoprecipitation buffer, and subjected to incubation with TRIB3 antibody for immunoprecipitation using agarose G-Plus beads. After verifying expression of TRIB3 by Western blot (Supplementary Fig. 2), the pulldown samples were submitted to the UAB Comprehensive Cancer Center Mass Spectrometry and Proteomics Shared Facility for protein mass spectrometry and to identify the binding protein partners of TRIB3. To perform cell toxicity assay, the MIO-M1 TRIB3-overexpressing cells were incubated in 3-(4,5-dimethylthiazol-2-yl)-2,5-diphenyl tetrazolium bromide (MTT) solution (0.5 mg/mL/well) for 4 h at 5% CO_2. Following MTT incubation, the cells were incubated with DMSO solution for 15 min. Cell survival was measured by estimating optical density at 570 nm using a microplate reader.

To generate hypoxic conditions, 24 h after transfection, MIO-M1 TRIB3-overexpressing cells were transferred to AnaeroGen W-Zip Compact bags for 48 h to maintain hypoxic conditions as previously reported, which generated 1% oxygenation, thus inducing hypoxia. Proteins were extracted using radioimmunoprecipitation buffer,

and TRIB3 (45 kDa), hypoxia-inducible factor-1α (HIF1α) (120 kDa), EGFR1 (170 kDa), GLUT1 (60 kDa), GFAP (50 kDa), and VEGF (21 kDa) were detected, with band-normalized intensities to actin (42 kDa). Secondary HRP goat anti-mouse and anti-rabbit antibodies and infrared goat anti-mouse and anti-rabbit antibodies were used for detection. Immunoblots were imaged and analyzed using the LI-COR imager system. Experiments with downregulation of HIF1α and EGFR in MIO-M1 hypoxic cells were conducted using respective siRNAs at a concentration of 100 nmol/L.

Glucose uptake assay was performed in MIO-M1cells transfected with siRNA *Hif1α* and exposed to hypoxia 24 h later. At 72 h post-transfection, the cells were taken out of the hypoxia bags and treated with florescent 2-deoxy-2-[(7-nitro-2,1,3-benzoxadiazol-4-yl) amino]-D-glucose (2-NBDG) for 30 min, as recommended by the manufacturer. Then, cells were washed with 1× analysis buffer, treated with trypsin, and resuspended in 400 μL of 1× analysis buffer. The glucose uptake was measured by flow cytometry using an LSRFortessa flow cytometer at the UAB Comprehensive Flow Cytometry Core. Confocal microscopy was used to obtain florescent images of cellular glucose uptake at 488 nm, and florescent signal was quantified using ImageJ software.

Statistics

Data were analyzed using either two-tailed unpaired Student *t* test or one-way or two-way ANOVA. Statistical significance was set at $P < 0.05$. The results were plotted in scatter plots to show individual data points and mean ± SEM as summary statistics using GraphPad Prism 8 software.

Data and Resource Availability

All data generated or analyzed during this study are included in the published article and its supplementary material.

RESULTS

In this study, we investigated the role of TRIB3 in the development and progression of human DR and leveraged STZ-injected and hypoxia-driven mouse models mimicking early molecular and advanced neurovascular pathophysiological complications of DR, respectively (19,20). First, we assessed the TRIB3 level in human diabetic retinas.

Human Diabetic Retinas Overexpress TRIB3 Protein

Recent studies conducted with diabetic animal models have clearly demonstrated associations between TRIB3 and numerous diabetes-associated complications, such as hyperhomocysteinemia (10,21) nonalcoholic fatty liver disease (22), diabetic nephropathy, and visceral obesity (23,24). Therefore, we tested the hypothesis that TRIB3 expression is also altered in hyperglycemic retinas. To this end, we analyzed and quantitated TRIB3 immunoreactivity in different human control (n = 5) and diabetic (n = 5) retinas. Overall, TRIB3 expression in analyzed diabetic retinas was more than threefold higher than control retinas (Supplementary Fig. 3). A representative diabetic retina of an 84-year-old man is shown in Fig. 1*A*. A strong signal for TRIB3 immunoreactivity was observed in retinal endothelial, ganglion, and photoreceptor cells compared with the control retina of an 82-year-old man without diabetes. Increased TRIB3 staining was observed. IHC analysis with antibody against CD31, a known endothelial cell marker, revealed the colocalization (in yellow) of TRIB3 (in red) and CD31 (in green) signals, suggesting expression of TRIB3 in endothelial cells of human diabetic retina. The hypertrophic blood vessel visualized by colocalization of TRIB3 and CD31 in human diabetic retinas is shown in Fig. 1*A*.

STZ-Induced Mouse Diabetic Retina and Hypoxic Müller Cells Demonstrate TRIB3 Overexpression

To proceed further, we took advantage of the TRIB3 KO mice and used both a pharmacological approach to induce hyperglycemia based on injection with STZ and a hypoxia-induced vascularization approach using an OIR model to mimic NPDR and proliferative retinopathy, respectively. RNA analysis of the retinas from mice at 4 weeks after STZ injection demonstrated an approximately fourfold upregulation of *Trib3* mRNA, suggesting that TRIB3 overexpression occurs early in the course of disease (Fig. 1*B*). TRIB3 expression level was also significantly upregulated in the hypoxic Müller MIO-M1 cells compared with normoxia on the basis of Western blot analysis (Fig. 1*C*), suggesting that hypoxia in human DR could upregulate TRIB3 expression level.

The results of the RNA and protein analyses were confirmed in mouse hyperglycemic and hypoxic retinas, which showed a strong immunoreactivity for TRIB3 in IHC (Fig. 1*D* and *E*). To verify that hyperglycemic RGCs overexpress TRIB3, we further performed an IHC analysis with antibody recognizing the RGC marker BRN3A and TRIB3 in control and STZ-treated retinas at 32 weeks (Fig. 1*F*). A colocalization shown in yellow was detected from TRIB3 (in red) and BRN3A (in green) signals, suggesting TRIB3 expression in hyperglycemic RGC. Given that TRIB3 reportedly controls insulin signaling and resistance in cells in general (25), we next tested the hypothesis that TRIB3 regulates glucose uptake and alters metabolic equilibrium in hyperglycemic retinas.

Hyperglycemic C57BL/6 Retinas Demonstrate Raised RGL, Whereas Hyperglycemic TRIB3 KO Retinas Manifest a Diminished Level of Glucose

Previously, it was reported that conventional TRIB3 KO in mice does not cause a significant difference in the BGL as a response to STZ injection compared with C57BL/6 mice (26). We confirmed this by detecting similar BGLs in both normal and diabetic C57BL/6 and

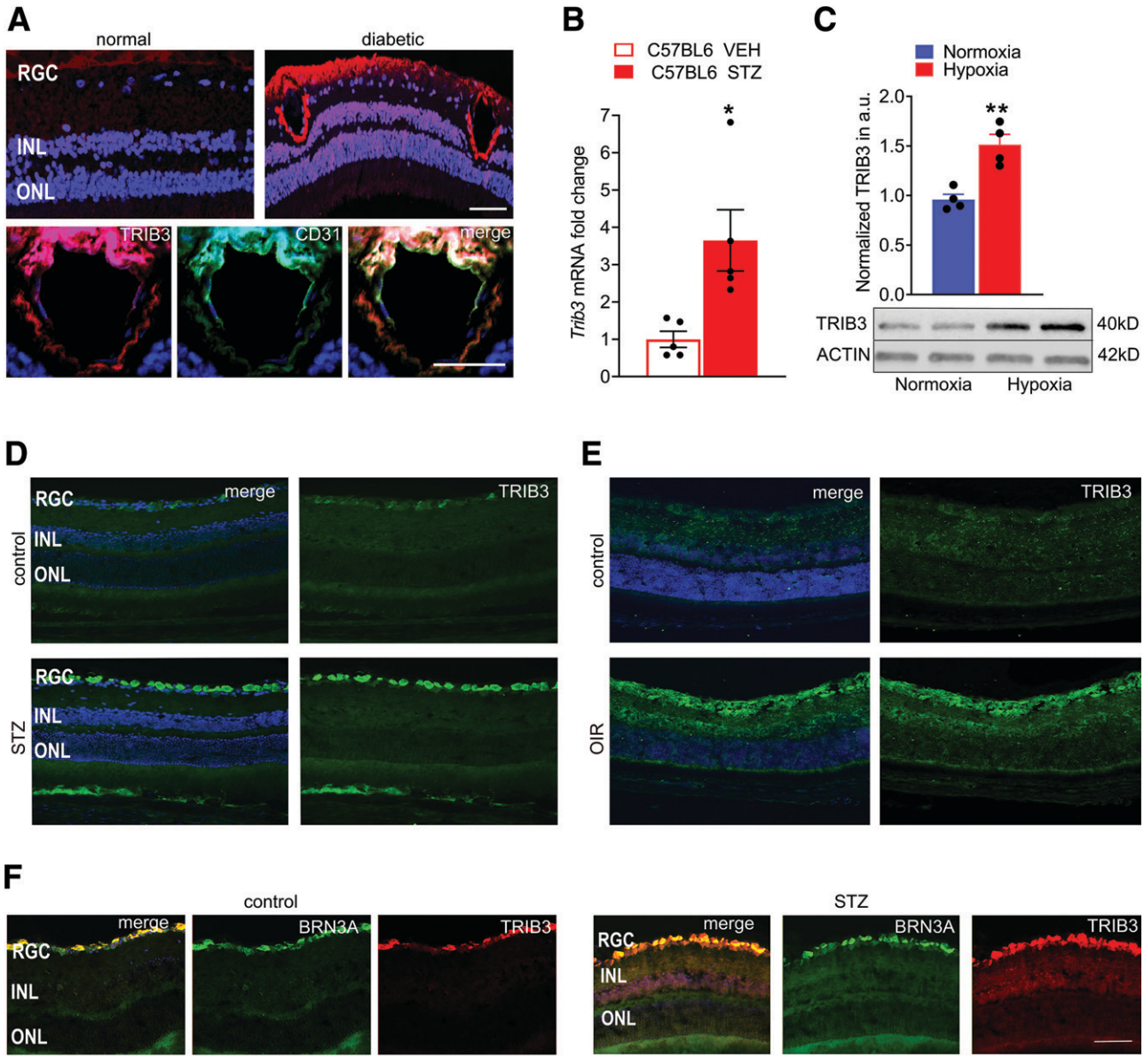

Figure 1—Human and mouse diabetic retinas overexpress TRIB3 protein. *A*: TRIB3 expression in the human diabetic retinas detected using IHC with anti-TRIB3 primary antibody is shown in red. Strong TRIB3 immunoreactivity is detected in the ONL, INL, RGC, and endothelial cells in the human diabetic retina. The TRIB3 immunoreactivity also colocalizes (in yellow) with $CD31^+$ cells (in green), suggesting that $CD31^+$ endothelial cells of the fibrovascular membrane also express TRIB3. Scale bar = 50 μm. *B*: Detection of TRIB3 expression in mouse diabetic retinas at 4 weeks of hyperglycemia by quantitative real-time PCR. Data are mean ± SEM (n = 5). *C*: TRIB3 overexpression detected in hypoxic Müller MIO-M1 cells at 48 h. *D*: Detection of TRIB3 in the mouse normal and diabetic retinas at 32 weeks after STZ-induced hyperglycemia (in green). DAPI-stained nuclei are shown in blue. Merged images are on the left. Robust TRIB3 expression is detected in the RGC layer. *E*: Detection of TRIB3 in normoxic and hypoxic mouse retina at P17. Robust TRIB3 expression is detected in the RGC, IPL, INL, and ONL (in green). DAPI-stained nuclei are shown in blue. Merged images are on the left. *F*: Expression of TRIB3 is colocalized with the RGC marker BRN3A in control and diabetic retinas at 32 weeks of hyperglycemia. TRIB3 is shown in red, BRN3A is shown in green, and colocalization is shown in yellow. DAPI-stained nuclei are shown in blue. Robust TRIB3 expression is detected in the RGC layer. Scale bar = 100 μm. $*P < 0.05$, $**P < 0.01$. a.u., arbitrary units; VEH, vehicle.

TRIB3 KO mouse groups (Supplementary Table 2). On the basis of this, we asked whether hyperglycemia also increased RGL. Using a calorimetric assay, we determined that 4-week hyperglycemic mice have a higher RGL than their nondiabetic controls. Interestingly, TRIB3-ablated hyperglycemic retinas demonstrated a significant reduction in RGL, despite the well-matched BGL (Fig. 2*A*). In agreement with the results of RGL analysis, hyperglycemic TRIB3 KO retinas also manifested significantly reduced *Glut1* mRNA expression (Fig. 2*B*). Given that the retina is extremely sensitive to glucose and that an excess of glucose in the retina may modify cellular metabolism, we analyzed early metabolic changes in hyperglycemic retinas.

Hyperglycemic TRIB3 KO Retinas Show Altered Metabolic Responses

TRIB3 is a known metabolic switcher responsible for moving cells from the homeostatic stage to metabolic dysfunction. Therefore, we analyzed the energy metabolism in 4-week diabetic retinas of mice mimicking early diabetic changes (19,20,27). We monitored both the cellular OCRs and the ECARs in a real-time experiment to measure the mitochondrial respiration and glycolysis rate in the retina using a Seahorse Extracellular Flux Analyzer (Fig. 2*C–I*). Extracellular acidification is derived from both lactate, produced by anaerobic glycolysis, and CO_2, produced in the citric acid cycle during respiration. However, a previous study revealed that retinas, manifesting the Warburg effect, convert 80–96% of glucose into lactate rather than fully oxidizing it to CO_2 in their mitochondria (28). Here, we found that the ECAR baseline was significantly higher in C57BL/6 diabetic retinas, whereas TRIB3 KO hyperglycemic retinas showed no differences compared with both controls (Fig. 2*C*). These results indicate a dramatic difference in acidification rate between C57BL/6 and TRIB3 KO diabetic retinas. In fact, the ECAR in the TRIB3 KO diabetic retinas dropped significantly as early as the first 10 min of the real-time experiment, and this decline continued over time. However, when we treated the retinal tissue with glucose, dramatic changes were observed in the ECAR of TRIB3 KO diabetic retinas. Although both C57BL/6 and TRIB3 KO diabetic retinas responded immediately to glucose, the TRIB3 KO hyperglycemic retinas demonstrated a more robust ECAR response at 45 min compared with ECAR at 40 min (approximately fivefold TRIB3 KO vs. twofold in C57BL/5, $P < 0.01$) (Fig. 2*D*). Further analysis of the post-glycolysis ECAR in C57BL/6 and TRIB3 KO diabetic retinas revealed that these tissues manifested a similar glycolysis rate (Fig. 2*E*). We next added oligomycin, a known inhibitor of mitochondrial ATP synthase and respiration, to the retinal preparations; this caused the overall glycolytic capacity to drop in a time-dependent manner in both C57BL/6 and TRIB3 KO diabetic groups (Fig. 2*F*). Although vehicle- and STZ-injected retinas responded similarly within a single mouse strain, a significant difference was observed between C57BL/6 and TRIB3 KO diabetic retinas: The glycolytic capacity in diabetic TRIB3 KO retinas was lower ($P < 0.01$).

The mitochondrial respiratory rate in the mice was measured with a mitochondrial stress test, and the OCR was recorded (Fig. 2*G*). The basal OCR was significantly lower in TRIB3 KO diabetic retinas than in C57BL/6 ($P < 0.0001$), suggesting that under hyperglycemic conditions, a basal mitochondrial respiration in hyperglycemic retinas could be controlled by TRIB3. In retinal samples stimulated by adding glucose, we observed a dramatic increase of OCR in TRIB3 KO (~1.5-fold in TRIB3 KO vs. 1.0-fold in C56BL/6, $P < 0.001$) (Fig. 2*H*). Time-dependent examination of the retinal tissue responses to glucose demonstrated that hyperglycemic TRIB3 KO retinas uniquely manifested significantly low OCR ($P < 0.05$) (Fig. 2*I*). Thus, our data demonstrate that TRIB3 ablation in the diabetic retinas manifests altered metabolic responses, which prompts a further exploration of whether other retinal cellular signaling systems are affected at early stages of DR development by TRIB3.

TRIB3 Ablation Reduces Inflammation in Diabetic Retinas

There is a growing literature suggesting that TRIB3 controls inflammatory response in cells (29). To verify the ability of TRIB3 to control the inflammatory response in the retina, mice injected with LPS were sacrificed after 24 h to analyze IBA1, a microglia/macrophage marker (Fig. 3*A*). IHC analysis demonstrated a dramatically reduced number of IBA1-positive cells in the retinas of LPS-injected TRIB3 KO mice, suggesting that TRIB3 ablation could be responsible for the modified proinflammatory response in the retina.

Given the early metabolic changes in diabetic retinas at 4 weeks, we analyzed the expression profile of the genes known to associate with DR, including *Hif1α*, *Aif1*, *Cox2*, *Icam1*, *Nf-kb*, *Rc3h1* (Roquin), *Zc3h12a* (Regnase or Mcp-1–induced protein-1), and *Vegf*. We found that TRIB3 ablation in diabetic retinas tremendously diminished expression levels of these genes. For example, expression of the intracellular adhesion molecule *Icam1*, responsible for communication between retinal endothelial cells and leukocytes in the diabetic eye, and COX2, a critical player in RGC survival (30), were dramatically reduced in TRIB3 KO diabetic retinas (Fig. 3*B*). These data indicate that TRIB3 ablation results in an altered inflammatory response in early diabetic retinas in addition to energy metabolism.

TRIB3 KO Prevents RGC, Endothelial Cell, and Pericyte Loss

RGC loss in the diabetic retina has been reported in the literature (31,32). At 32 weeks of hyperglycemia, we assessed the RGC function and viability in the retinas and found that although the C57BL/6 diabetic retinas demonstrated significant loss of RGC, TRIB3 ablation protected hyperglycemic retinas from RGC death. The number of RGCs calculated within 100-μm distance in the retinas of TRIB3 KO diabetic mice were comparable to those found in control C57BL/6 mice (Fig. 4*A* and *B*). Therefore, we next recorded the PhNR amplitudes to measure the RGC function known to detect early neuronal damage in human and mouse retinas (32,33). Interestingly, the RGC loss in C57BL/6 hyperglycemic retinas correlated with dramatic functional loss as measured by PhNR recording, whereas decline in PhNR was remarkably prevented in TRIB3 diabetic retinas (Fig. 4*C* and *D*).

The RGC layer in the eye is traversed by the retinal capillary beds at varying levels that provide nourishment for both the RGCs and the RGC axons (34). Therefore, given that DR is a vascular disease, we next assessed the role of TRIB3 in retinal endothelial cell health in diabetes. In the hyperglycemic retinas, we observed a dramatic

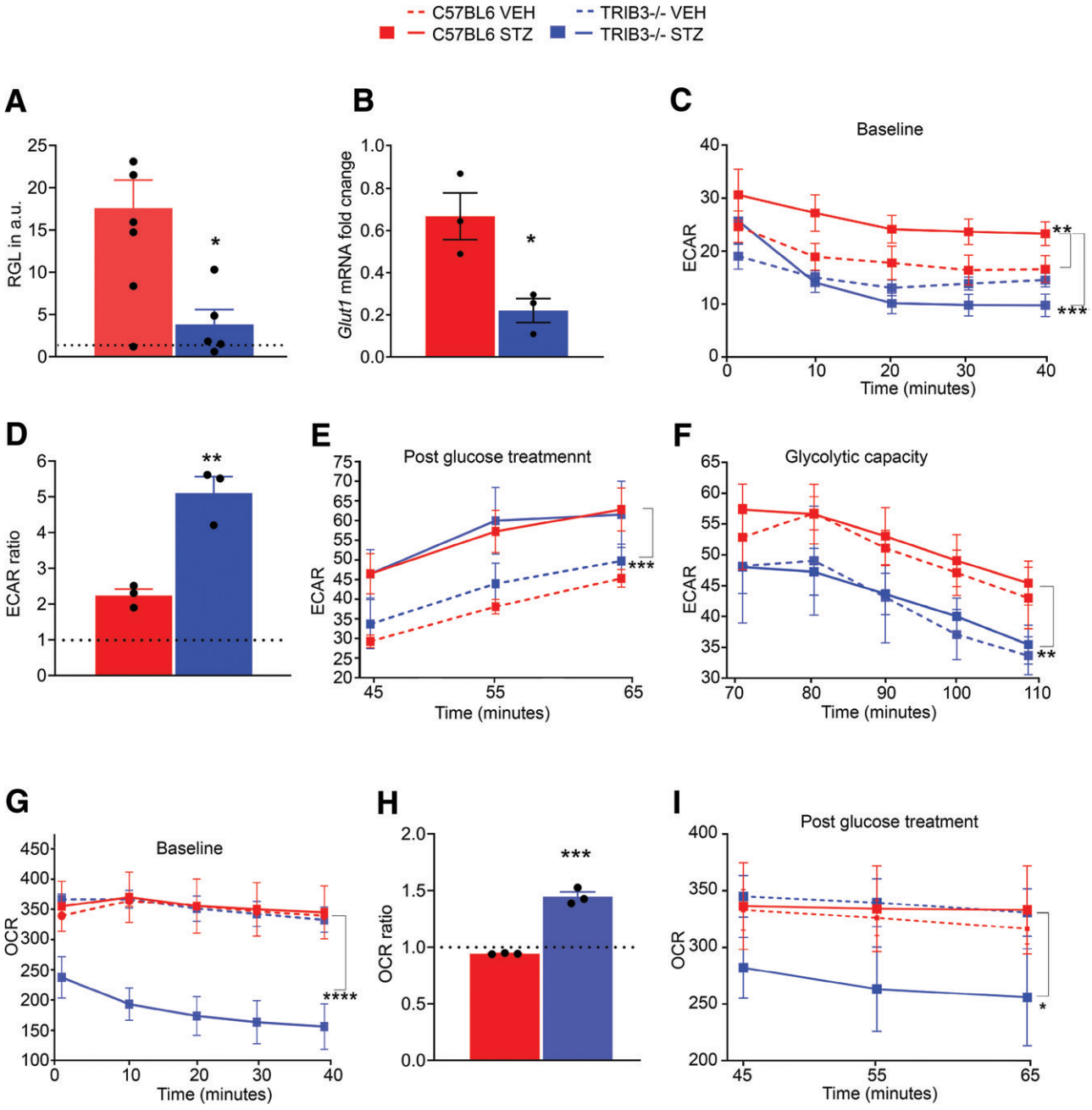

Figure 2—TRIB3 reprograms glucose metabolism in diabetic retinas. *A*: RGLs measured in diabetic retinas (mg/dL) were normalized to their appropriate controls (dotted line) at 4 weeks of hyperglycemia. Significant reduction of RGL is observed in TRIB3 KO diabetic retinas (C57BL/6 diabetic and control, n = 8–9; TRIB3 KO diabetic and control, n = 5–11). Also see Supplementary Table 2. *B*: TRIB3 controls expression of *Glut1* gene at 4 weeks of hyperglycemia (n = 3). Fold changes for each diabetic group were normalized to own controls. Significant reduction in *Glut1* expression is observed in TRIB3 KO diabetic retinas. *C–F*, *H*, and *I*: Results of the metabolic stress experiments (n = 4–6). *C*: The ECAR baseline of diabetic and control C57BL/6 and TRIB3 KO groups at 4 weeks postinjection (mpH/min). Significant increase in the ECAR baseline in C57BL/6 diabetic retinas is shown during the first 40 min. *D*: Addition of glucose results in dramatic jumps in the ECAR. Thence, the TRIB3 KO diabetic retinas manifest more sensitivity than C57BL/6 hyperglycemic tissue. The presented ECARs are expressed as the ratios of the normalized ECARs at 45 min over the normalized ECARs measured at 40 min (dotted line). *E*: Rates of glycolysis in the four experimental groups measured after glucose treatment in a real-time experiment. Both diabetic retinas demonstrate comparable levels of glycolysis. *F*: Measurement of glycolytic capacity in diabetic retinas after suppression of the mitochondrial respiration rate by using oligomycin. Reduced glycolytic capacity of TRIB3 KO diabetic retinas (∼18%) vs. C57BL/6 hyperglycemic retinas (mpH/min). *G*: The OCR baseline measurements in normal and diabetic mouse groups. Significant reduction in the OCR is detected in TRIB3 KO hyperglycemic retinas. *H*: Addition of glucose at 40 min results in a high sensitivity of the OCR in TRIB3 diabetic retinas registered at 45 min (dotted line). *I*: However, this jump does not cause an increase in the OCR compared with C57BL/6 diabetic retinas in a timely manner. The OCR continues to decline in TRIB3 diabetic retinas as measured in pmol/min. Data are mean ± SEM. *$P < 0.05$, **$P < 0.01$, ***$P < 0.001$, ****$P < 0.0001$. a.u., arbitrary units; VEH, vehicle.

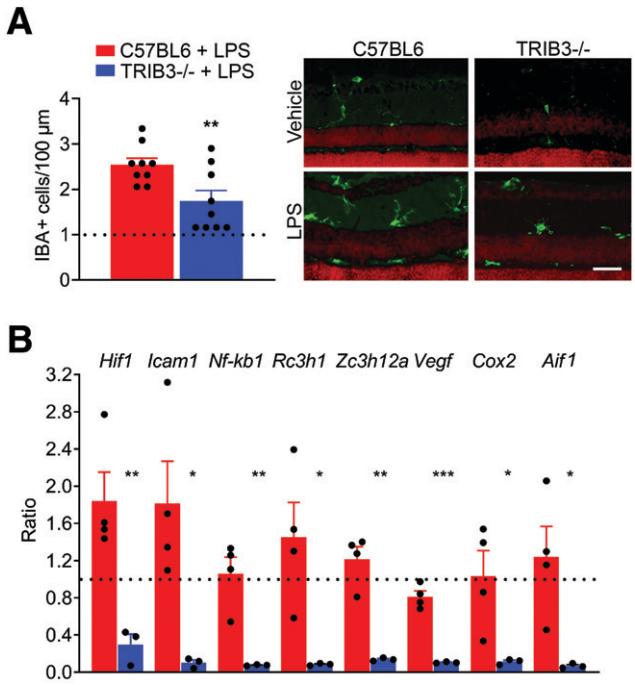

Figure 3—TRIB3 controls immunoresponse in stressed and diabetic retinas. *A*: Mice were intraperitoneally injected with 10 μL/g LPS and sacrificed 24 h later (n = 5). The cryostat retinal sections were subjected by IHC analysis with anti-IBA1 antibody, and IBA-positive cells per 100 μm were counted (in green). The results are presented as ratios of cells detected in LPS-injected retinas normalized to own controls (dotted lines). Scale bar = 100 μm. *B*: TRIB3 controls expression of proinflammatory genes at 4 weeks of hyperglycemia (n = 3–4). Fold changes for each diabetic group were normalized to own controls. Thus, we observe a dramatic decline in *Hif1α*, *Icam1*, *Nf-kb1*, *Rc3h1*, *Zc3h12a*, *Vegf*, *Cox2*, and *Aif1* expression in TRIB3 KO diabetic retinas. Data are mean ± SEM. *$P < 0.05$, **$P < 0.01$, ***$P < 0.001$.

cytoprotective effect of TRIB3 ablation. The pericyte loss observed in C57BL/6 retinas was reversed, and the increase in acellular capillaries was averted in TRIB3 KO diabetic retinas (Fig. 4*E*–*G*). Cumulatively, these results indicate that TRIB3 ablation not only has a neuroprotective effect on RGC but also maintains retinal vascular homeostasis in diabetic mice.

TRIB3 Ablation Manifests Reduced Vascular Dysfunction, Gliosis, and Overall Retinal Integrity Loss in Hypoxic Retinas

Previously, we reported that ATF4 downregulation is a therapeutic for hypoxic retinas and leads to dramatic reduction in NV and increase in the acellular area of OIR mice (35). TRIB3 is a downstream target of ATF4, the expression of which is upregulated during endoplasmic reticulum stress (36). It has also been suggested that hypoxic conditions upregulate Trib3 expression in retinal Müller cells (37). Thus, we explored hypoxic TRIB3-ablated retinas using the OIR model.

At P13, 1 day after the removal of pups from the oxygen chamber, VEGF expression was high in the C57BL/6 retinas, as expected. Surprisingly, however, TRIB3 ablation in hypoxic retinas resulted in a reduced VEGF level (Fig. 5*A*). For example, C57BL/6 hypoxic retinas normalized to the control demonstrated a 1.3-fold increase in VEGF, whereas normalized TRIB3 KO OIR showed a substantial decline in VEGF expression. Therefore, learning about TRIB3-mediated control of VEGF in the wild-type retina, we further analyzed VEGF-induced NV in OIR mice.

Analyses of the areas of NV and VO in the OIR retinas demonstrated that TRIB3 ablation significantly reduced formation of neovascular tufts (Fig. 5*B*, left graph and bottom images with the area specified in red). Hypoxic TRIB3 KO retinas manifested levels of VO similar to those found in C57BL/6 hypoxic tissues (Fig. 5*B*, right graph and bottom images with the area specified in yellow). This difference in NV prompted the question of whether TRIB3-mediated vascularization causes the compromise of retinal integrity and morphology observed in C57BL/6 OIR retinas.

Interestingly, TRIB3 KO in hypoxic retinas preserved overall retinal integrity. Although the C57BL/6 OIR retinas demonstrated reduced INL, IPL, and OPL thicknesses, TRIB3 KO dramatically reversed these structural changes; no differences were observed between TRIB3 KO OIR and normoxic C57BL/6 or TRIB3 retinas (Fig. 6*A*).

Müller cells are known to play a pivotal role in the development of DR and respond promptly to hyperglycemia and hypoxia (38). Therefore, we examined Müller cells in hypoxic retinas by detecting the colocalization of GFAP and vimentin, known glial cell markers. We found that the TRIB3 KO hypoxic mice demonstrated a significantly lower Müller cell immunoreactivity compared with C57BL/6 OIR retinas (Fig. 6*B*). Moreover, detection of the GFAP level in TRIB3 KO OIR mice by Western blot also indicated a dramatic reduction in the overall expression, supporting the observation of diminished gliosis in hypoxic TRIB3 KO retinas (Fig. 5*C*). Together, these results show that TRIB3 not only is involved in early metabolic and inflammatory changes but also may contribute to the progression of DR.

TRIB3 Controls Glucose Signaling and VEGF Expression, Overall Affecting Retinal Cell Viability

We next investigated the mechanism of TRIB3-mediated control of the development and progression of DR in vitro. Given that Müller cells demonstrated high immunoreactivity in OIR C57BL/6 retinas and could be the sources of VEGF and proinflammatory cytokine expression, we further performed tissue culture experiments with MIO-M1 cells.

The molecular mechanisms of DR are complex and multifactorial. Early molecular changes in diabetic retinas have been reported to occur through a compromised AGE pathway. Therefore, using Müller cells, we asked whether the treatment of MIO-M1 cells with 500 mmol/L AGE

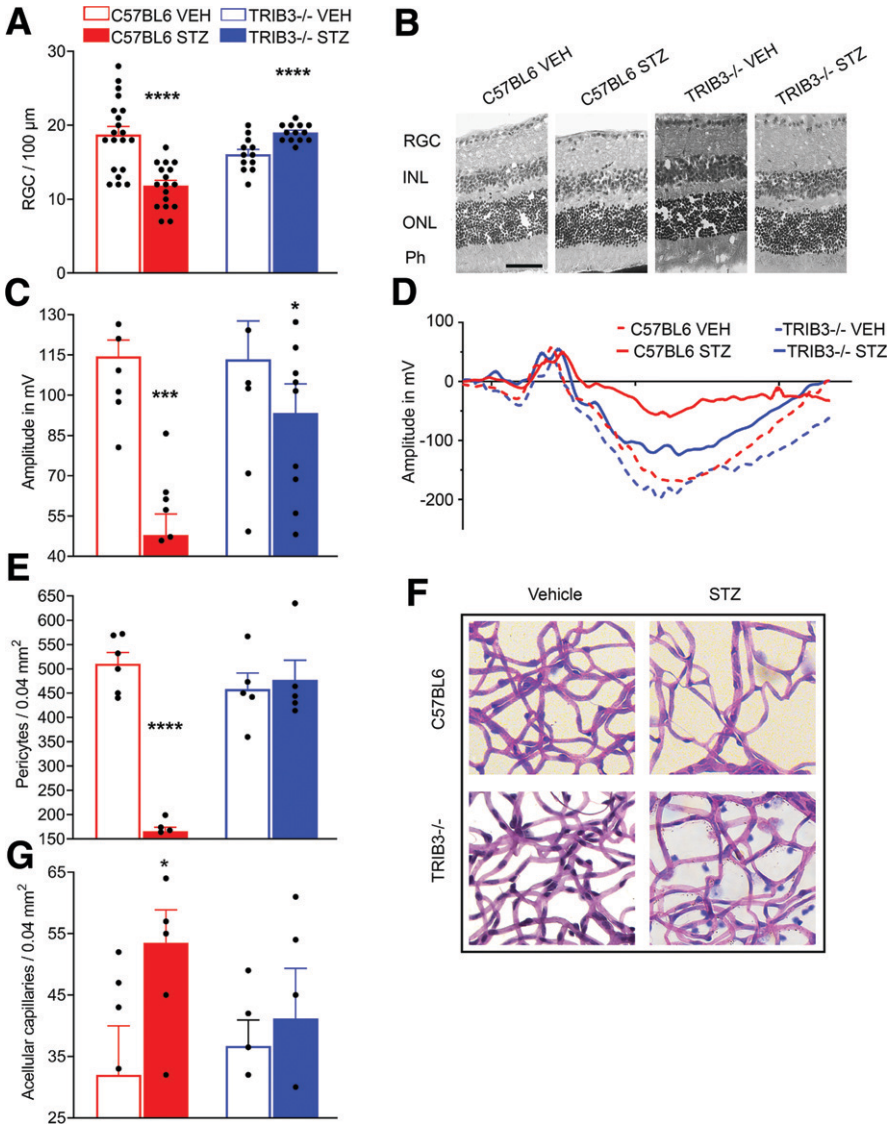

Figure 4—TRIB3 controls neuronal and endothelial health in diabetic retinas at 32 weeks after STZ administration. *A*: The number of ganglion cells/100 µm is dramatically increased in the diabetic TRIB3 KO mouse retinas compared with the diabetic C57BL/6 group. No changes were observed between control C57BL/6 and control TRIB3 KO retinas and control TRIB3 KO and diabetic TRIB3 KO retinas, while a significant difference was detected between control and diabetic C57BL/6 groups ($n = 6$). *B*: Representative images of the hematoxylin-eosin–stained control and diabetic retinas. Scale bar = 100 µm. *C*: The PhNR amplitudes characterizing the RGC function as recorded by the photopic electroretinography procedure in the C57BL/6 control and diabetic ($n = 9$ for both) and TRIB3 KO control and diabetic ($n = 8$–12) mouse groups. Significant diminishing of the RGC function is detected in the C57BL/6 diabetic mice, whereas dramatic elevation of PhNR is observed in TRIB3-ablated diabetic retinas. *D*: Representative images of PhNR registered in all four groups. *E*: The number of pericytes detected in a 0.04-mm^2 area of the retina is markedly reduced in the diabetic C57BL/6 retinas compared with other mouse groups ($n = 6$ for C57BL/6 control and diabetic mice, $n = 5$ for TRIB3 KO control and diabetic mice). TRIB3 ablation slows down the pericyte loss in diabetic retinas. *F*: TRIB3 ablation in diabetic retina prevents formation of acellular capillaries detected in a 0.04-mm^2 area of the retina. *G*: Representative images for periodic acid Schiff–stained retinal pericytes and acellular capillaries in the retinas of the four mouse groups. Data are mean ± SEM. *$P < 0.05$, ***$P < 0.001$, ****$P < 0.0001$. Ph, photoreceptor; VEH, vehicle.

induces TRIB3 overexpression. The results demonstrated significant upregulation of TRIB3 in 48 h (Fig. 7*A*). These data concord with the results obtained in STZ-induced hyperglycemic mice and the hypoxia-treated MIO-M1 cells, indicating that in diabetic hypoxic retina, TRIB3 could be overexpressed earlier in the course of disease. Besides overexpression of TRIB3 in hypoxic MIO-M1 cells, we also identified occurrence of overexpression of HIF1α and EGFR (Fig. 7*B*). The choice of the validated proteins was determined by the literature, and the results obtained in hyperglycemic mouse retina and MIO-M1 cells overexpressing TRIB3 (Supplementary Fig. 2). Thus, similar to hyperglycemic retinas, hypoxia in MIO-M1 cells induced both TRIB3 and HIF1α.

Interestingly, TRIB3 by itself can compromise MIO-M1 cell viability (Fig. 7*C*); more prominent cell death was

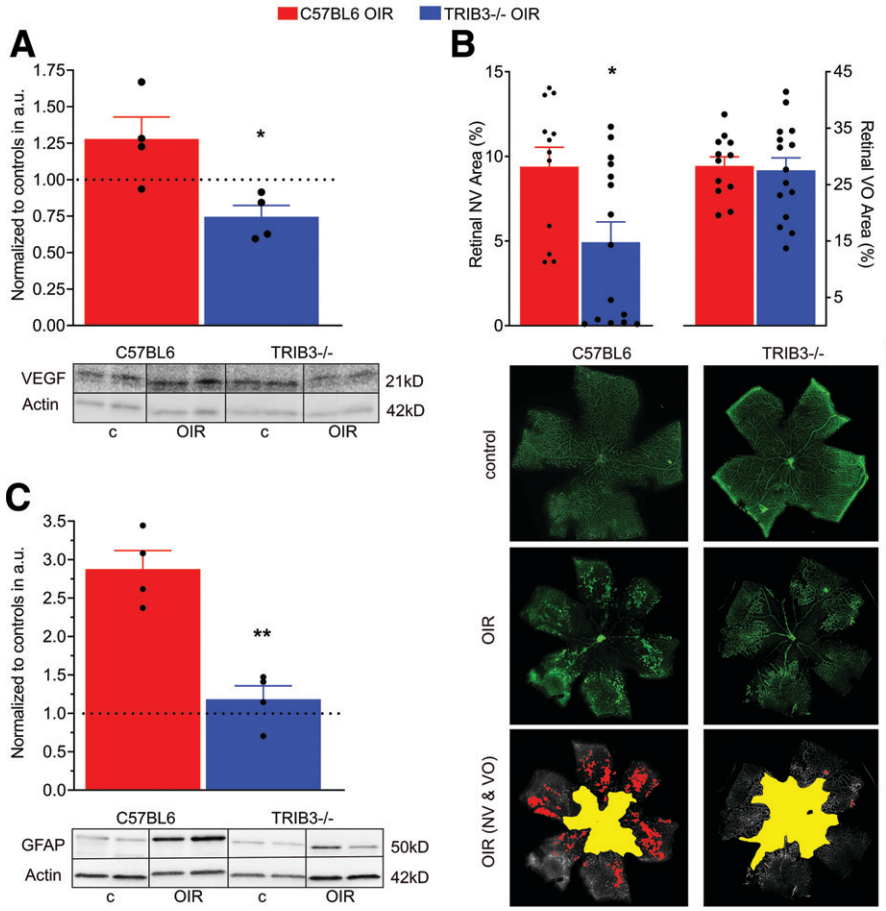

Figure 5—TRIB3 promotes retinal vascularization during hypoxia. *A*: Expression of VEGF normalized to own controls (dotted line) in two hypoxic groups at P13 ($n = 4$). Significant reduction of VEGF in TRIB3 KO hypoxic retinas is observed. Representative images of the Western blots probed with anti-VEGF antibody are shown at the bottom. *B*: Ratios of the NV (left) and VO (right) areas in the hypoxic C57BL/6 and TRIB3 KO retinas ($n = 6–8$) to the whole retinal areas at P17. The flat mount images were used to run a computer program developed by Xiao et al. (17) to analyze areas of NV and VO. Significant reduction in NV area is observed in hypoxic TRIB3 KO retinas of pups, while no changes in VO between OIR C57BL/6 and TRIB3 are detected. Representative images for NV and avascular area in the flat mount retinas of pups were stained with isolectin (in green). *C*: Expression of GFAP in two diabetic C57BL/6 and TRIB3 KO groups normalized to own controls (dotted line) at P13 ($n = 4$). A dramatic reduction in the GFAP level in diabetic retinas with TRIB3 ablation was detected. Representative images of the Western blots probed with anti-GFAP antibody are shown at the bottom. Data are mean ± SEM. $^*P < 0.05$, $^{**}P < 0.01$. a.u., arbitrary units; c, control.

found in MIO-M1 transfected with TRIB3-DDK plasmid than in control cells. These results are comparable with the RGC loss observed in hypoxic diabetic retinas overexpressing TRIB3. Given that HIF1α and EGFR along with TRIB3 were overexpressed in cultured Müller cells, we investigated whether TRIB3 is an upstream mediator of these proteins by using TRIB3 overexpression. In hypoxic Müller cells overexpressing TRIB3-DDK cDNA, HIF1α and EGFR were upregulated along with increased GFAP, VEGF, and GLUT1 proteins, indicating that TRIB3 controls these protein expressions as well (Fig. 7*D*). In hypoxic MIO-M1 cells treated with siRNA targeting *HIF1α*, we found that the levels of EGFR, GLUT1, and VEGF were significantly lower, whereas GFAP was unresponsive to the knockdown of *HIF1α*. This suggests that GFAP may be directly regulated by TRIB3, and its expression is not HIF1α dependent (Fig. 7*E*).

Given that TRIB3 expression is hypoxia induced and TRIB3, in turn, regulates HIF1α expression leading to changes in GLUT1 (Fig. 7*E* and Supplementary Fig. 4), we asked whether *Hif1α* detected in C57BL/6 hyperglycemic retinas (Fig. 3*B*) could be responsible for the glucose uptake in Müller cells. Particularly, the observation of higher RGL in hyperglycemic C57BL/6 retinas overexpressing *Hif1α* mRNA was worth further investigation. Therefore, we treated hypoxic Müller cells transfected with control or *HIF1α* siRNAs with a fluorescent glucose analog, 2-NBDG, known to inhibit glycolysis via its action on hexokinase and analyzed levels of fluorescence using flow cytometry and confocal microscopy (Fig. 8*A* and *B*, respectively). We observed a significant reduction in glucose uptake that occurred in HIF1α-dependent manner. Given that TRIB3 overexpression leads to an increase in HIF1α protein level and *Hif1α* knockdown diminishes

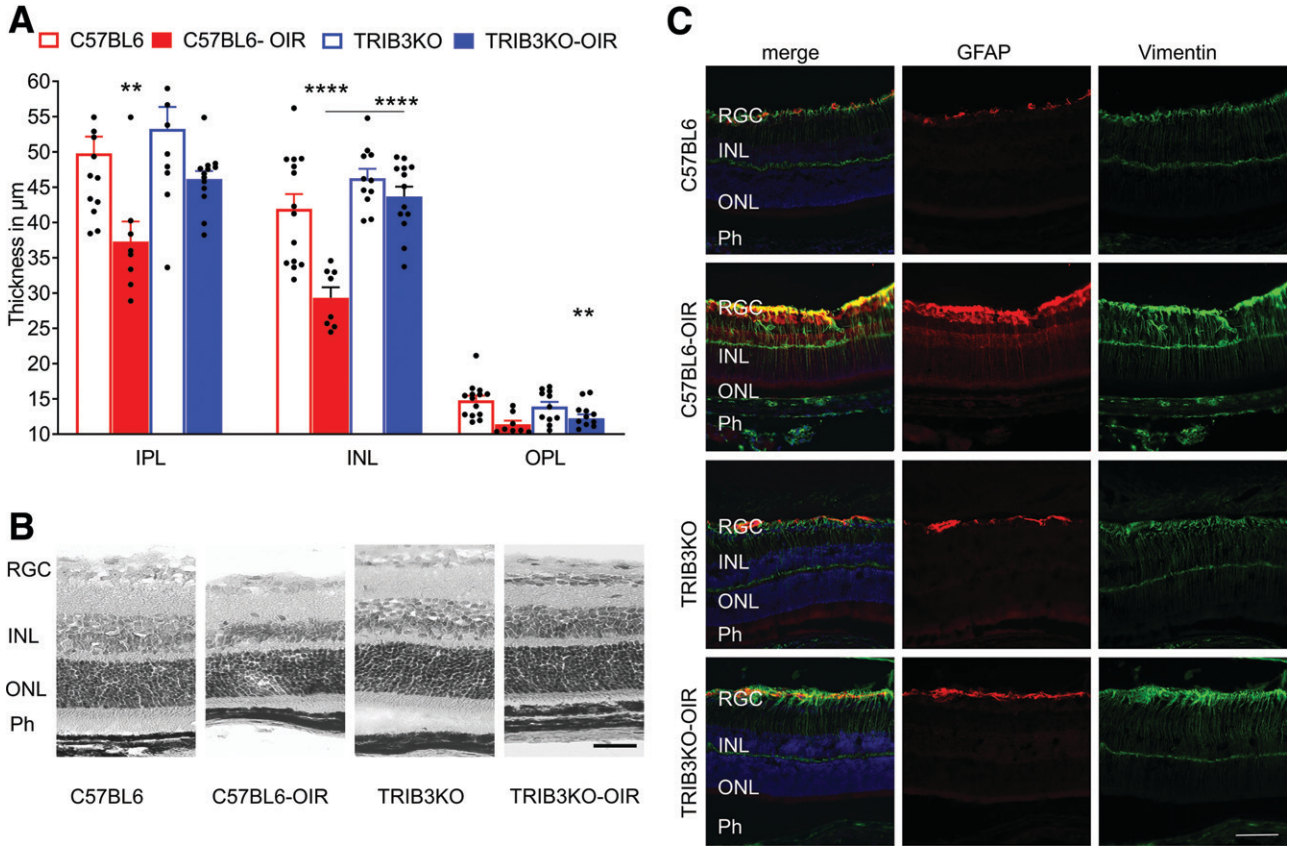

Figure 6—TRIB3 promotes retinal integrity loss and activates gliosis during hypoxia. *A*: TRIB3 KO significantly preserves the retinal integrity in hyperglycemic mice (n = 5). The IPL, INL, and OPL thicknesses are diminished in C57BL/6 diabetic retinas, whereas protection is observed in TRIB3 KO diabetic retinas, demonstrating no difference compared with control retinas in both genetic groups. *B*: Representative images of the hematoxylin-eosin–stained retinas in the four mouse groups. *C*: Representative images of the retinal sections probed with anti-GFAP (red) and anti-vimentin (green) antibodies and DAPI (blue) in the four mouse groups taken with fluorescent microscopy. Merged images are shown on the left. Scale bars = 100 µm. Data are mean ± SEM. $^{**}P < 0.01$, $^{****}P < 0.0001$. Ph, photoreceptor.

glucose uptake in hypoxic Müller cells, we next wondered whether downregulation of *Trib3* by itself can compromise the level of glucose uptake in hypoxic cells. Thus, in hypoxic Müller cells cotransfected with TRIB3-DDK cDNA and antisense oligos targeting *Trib3,* we found that a 60% reduction in TRIB3 protein results in a 21% reduction in 2-NBDG uptake (Supplementary Fig. 5). These results suggest that the glucose uptake in these cells and the metabolic changes in hyperglycemic retinas could be regulated through a TRIB3→HIF1α axis. Altogether, these findings indicate that TRIB3 is upstream of HIF1α, EGFR, and GFAP, which allows this molecule to control glucose metabolism, cytokine expression, angiogenesis, and gliosis in retinal cells.

DISCUSSION

Overall, the molecular mechanisms of DR are complex and multifactorial. Hyperglycemic conditions affect the intracellular glucose level, leading to the retinal endothelial and neuronal cells failing to properly regulate cellular metabolism. Early molecular changes in diabetic retinas have been reported to occur through a compromised polyol pathway, protein kinase C pathway, AGE pathway, and hexosamine biosynthetic pathway in retinal cells (39). Besides the dysregulation of these cellular pathways, hypoxia-induced HIF1α and VEGF overexpression plays key roles in the progression of NDPR to PDR (1,40). In contrast, little is known about how early molecular changes occurring in diabetic retinas lead to the subsequent progression of the disease. Here, we present evidence confirming the critical role of TRIB3 overexpression during the development and progression of DR. First, we found that TRIB3 was overexpressed in human diabetic retinas and retinas of mice mimicking NPDR and proliferative retinopathy in patients, which provided a rationale to further investigate the role of TRIB3 in diabetic retinas. We discovered that TRIB3 overexpression induced HIF1α-mediated changes in GLUT1 level, glucose uptake, and VEGF expression. In addition, we observed that TRIB3 controlled EGFR expression. Finally, we determined that TRIB3 ablation in hyperglycemic and hypoxic retinas dramatically prevented retinal neuronal cell functional deficit and loss as well as VEGF-induced NV.

Retinal vascular homeostasis becomes compromised with the disease progression. PDR is characterized by

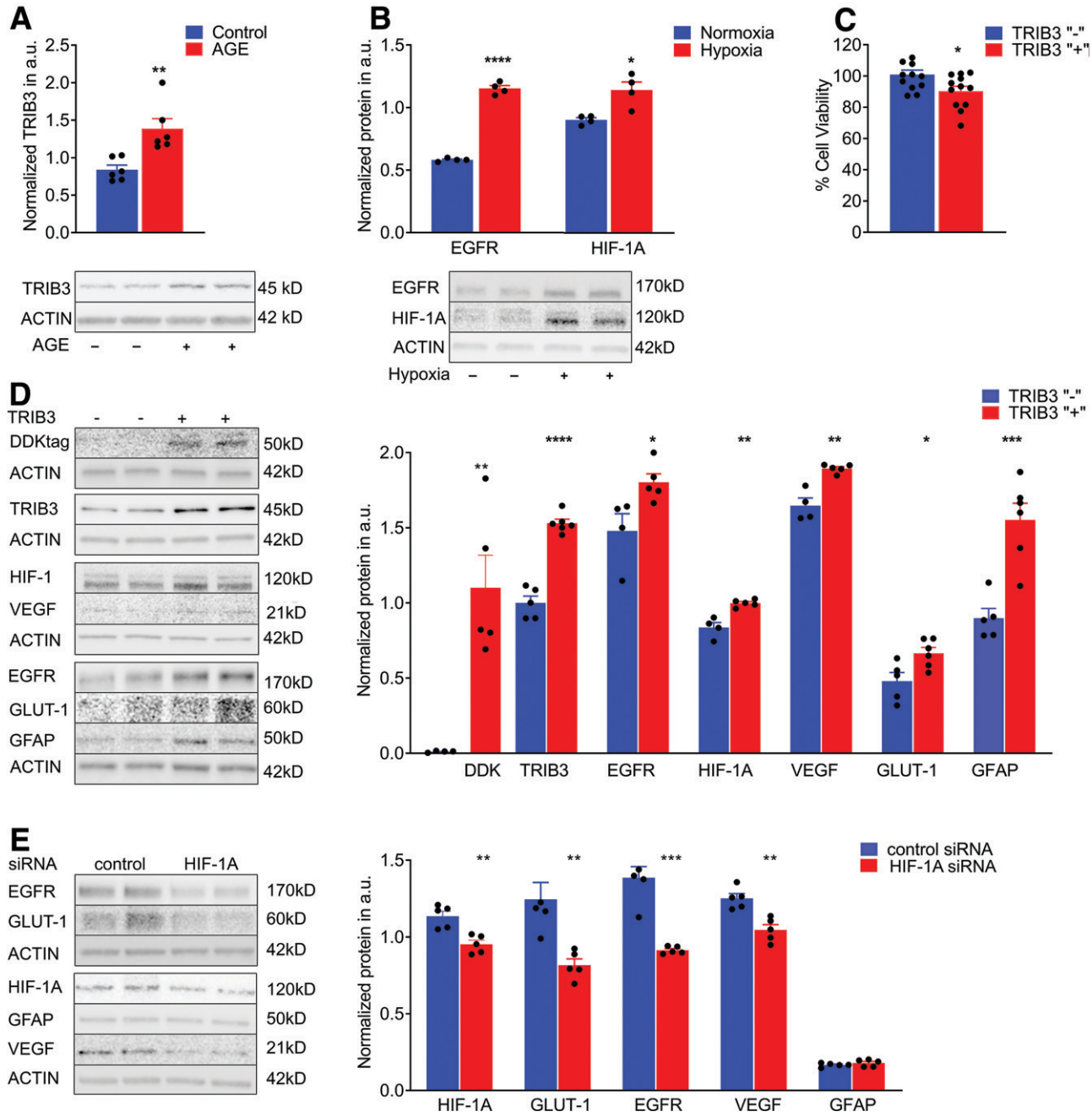

Figure 7—TRIB3 overexpression activates downstream signaling in Müller MIO-M1 cells. *A*: AGE treatment results in TRIB3 overexpression in 72 h (n = 6). *B*: Hypoxia induces HIF1 and EGFR protein in addition to TRIB3 (Fig. 1) (n = 4). *C*: Müller cells overexpressing TRIB3 demonstrate compromised cell viability (n = 4). *D*: Overexpression of TRIB3 in hypoxic Müller cells results in overexpression of EGFR1, HIF1α, VEGF, GFAP, and GLUT1 (n = 4–5). *E*: Knockdown of *Hif1a* mRNA in hypoxic Müller cells results in downregulation of GLUT1, EGFR1, and VEGF1, whereas GFAP expression does not respond to the treatment with siRNA (n = 5). Data are mean ± SEM. *$P < 0.05$, **$P < 0.01$, ***$P < 0.001$, ****$P < 0.0001$. a.u., arbitrary units.

uncontrolled growth of fragile blood vessels that can protrude and leak into the vitreous, causing blurry vision. This phenomenon is triggered by hypoxia in the retina, one of the known molecular inducers of NV. One of the interesting findings of our study is that both hypoxia and AGE conditions found in patients with diabetes caused the upregulation of TRIB3, which in turn controlled glucose metabolism, vascular function, and gliosis. Thus, our in vitro study indicated that HIF1α upregulation in diabetic retinas occurs in a TRIB3-dependant manner (Figs. 3 and 7). A previous study demonstrated that HIF1α induced TRIB3 overexpression (41). In fact, the HIF1α-TRIB3 relationship could be more delicate, and the regulation of their expressions may be interactive. For example, one such regulation is mediated through ATF4 transcriptional factor, which reportedly cooperates with both

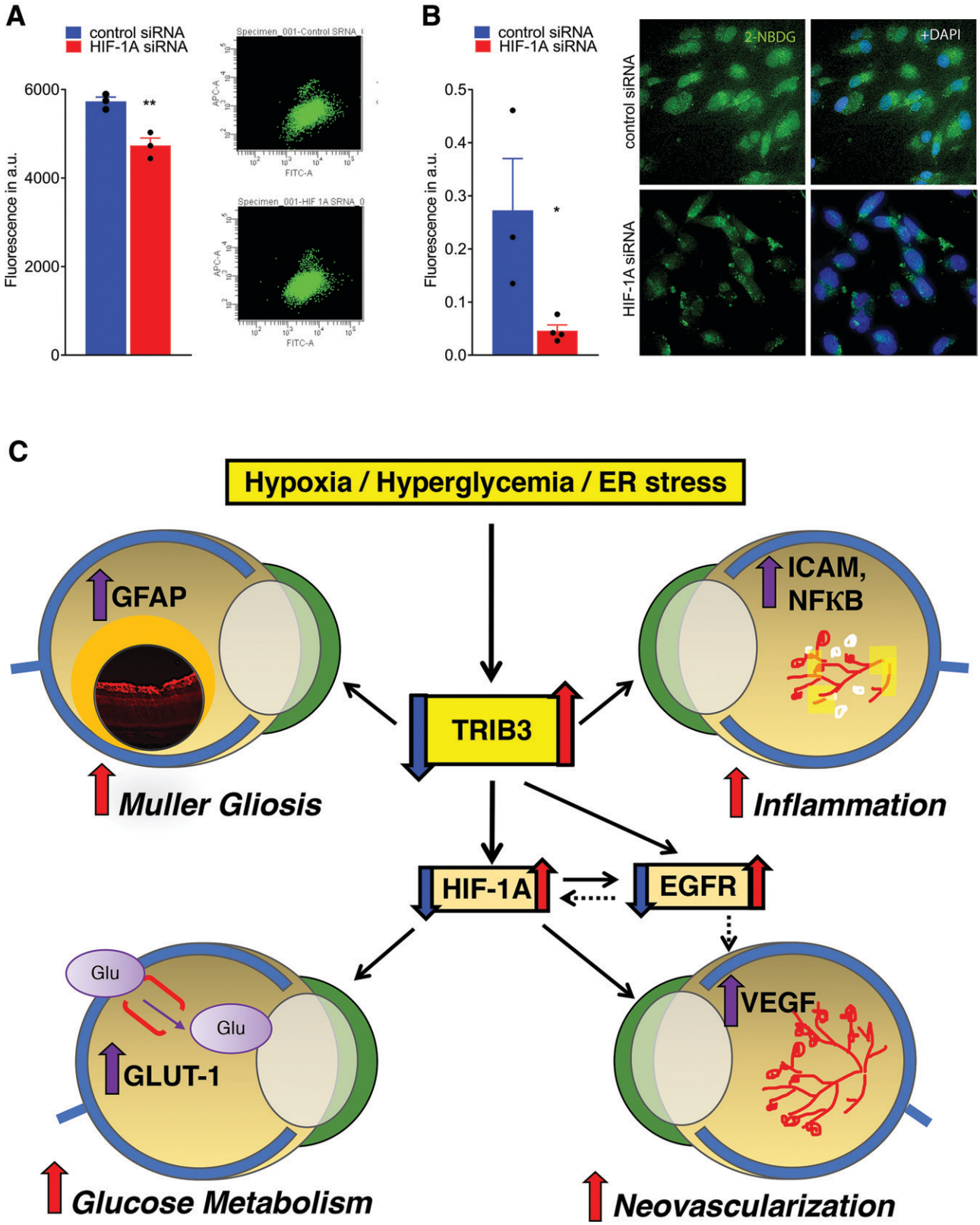

Figure 8—Treatment of hypoxic Müller cells with siRNA targeting *HIF1α* results in reduction of GLUT1 and fluorescent signal from 2-NBDG cellular uptake. *A*: Reduction of fluorescent signal from 2-NBDG uptake measured by flow cytometry ($n = 3$). *B*: Reduction of fluorescent signal from 2-NBDG cellular uptake registered in fixed cultured MIO-M1 cells using microscopy ($n = 3–4$). The calculation of fluorescent signal was performed using ImageJ. *C*: Schematic presentation of the proposed molecular mechanism of DR controlled by TRIB3. Under hyperglycemic and hypoxic conditions, TRIB3 overexpression leads to upregulation of HIF1α, EGFR, and GFAP. HIF1α overexpression results in GLUT1 activation followed by an increase in retinal glucose flux, overall affecting retinal metabolism.

proteins by inducing TRIB3 expression (36) and binding to HIF1α (42). The results of our in vivo study are in agreement with those obtained with HIF1α knockdown in hypoxic Müller cells. Although the HIF1α knockdown was not dramatic in this study, it seems sufficient to provide downstream cellular alterations, such as GLUT1 and glucose uptake, in cells during hypoxia. One of the plausible explanations for this phenomenon is that hypoxia and oxidative stress elevate HIF1α mRNA levels transcriptionally, likely through the NF-κB and Egr1 transcription factors at work. Under normoxic conditions, the half-life of HIF1α protein is very short (i.e., ∼5 min), and HIF1α rapidly degrades by hydroxylation at conserved prolyl and asparagine residues targeting it for degradation. During hypoxia, these hydroxylases are quickly inhibited, leading to the rapid and robust stabilization of HIF1α and, therefore, an altered half-life for the protein (43,44).

Recently conducted studies in cultured L6 myocytes (25,45) indicated that TRIB3 overexpression is induced in a glucose-dependent manner, resulting in reduced mitochondrial glucose oxidation and the maximal uncoupled OCR. Hence, it noteworthy to find that TRIB3 can regulate glucose uptake in diabetic retina and that this regulation occurs via HIF1α-mediated GLUT1 expression. Indeed, in the whole-retina samples, we found that TRIB3 ablation may modify glucose flux and *Glut1* expression and define glycolytic capacity of diabetic retina. C57BL/6 diabetic retinas presented higher RGL, confirming a previous study that reported an increase in glucose uptake in diabetic rat retinas (46). Changes in glucose flux and in RGL between C57BL/6 and TRIB3 KO diabetic retinas suggest a plausible explanation: reduction in glucose transporter GLUT1, detected in TRIB3 KO diabetic retinas, could be one reason.

TRIB3 KO in diabetic retinas may cause a metabolic shift that allows this retina to function under a "safe operating mode." Previously, it has been demonstrated that diabetic retinas may have higher lactate-pyruvate ratios, suggesting that elevated glucose level mimics the effects of hypoxia on glycolysis and cytosolic-free NADH/NAD^+ (47,48). These results were very similar to those observed in this study. C57BL/6 diabetic retinas had a higher baseline ECAR derived from lactate produced by anaerobic glycolysis. Although overall glycolytic capacity in the TRIB3 KO diabetic retinas was lower, the response of the retinas to glucose treatment was significantly higher in these mice. Interestingly, the TRIB3 KO diabetic retinas also displayed a lower OCR at baseline and revealed a higher sensitivity of the mitochondrial respiration rate in response to glucose treatment. Altogether, these results imply that TRIB3 KO hyperglycemic retinas might respond to glucose elevation similarly to C57BL/6 hyperglycemic retinas but operate at limited metabolic mode by reducing glucose flux instead.

EGFR reportedly promotes angiogenesis, cell proliferation, metastasis, and apoptosis in DR, and the inhibition of EGFR signaling protects diabetic retina from insulin-induced vascular leakage (49,50). Although we did not asses the level of EGFR in diabetic retinas, we found that TRIB3 overexpression observed in hypoxic MIO-M1 cells induces EGFR, suggesting that C57BL/6 diabetic retinas may also manifest EGFR increase. Moreover, the TRIB3-mediated EGFR increase could occur through HIF1α. Published reports indicated that the relationship between HIF1α and EGFR is reciprocal and that they can induce expression of each other in hypoxic conditions (51). Therefore, future experiments that investigate the TRIB3→EGFR→VEGF operating arm in diabetic retinas should be conducted to overcome limitations of the current study (Fig. 8*C*). Given the fact that diminished HIF1α level resulted in reduced VEGF, our data indicate that in hyperglycemic and hypoxic retinas, the observed correlation between TRIB3 and VEGF is promoted mostly through TRIB3→HIF1α signaling. Future experiments that investigate the TRIB3→EGFR→VEGF operating arm in diabetic retinas should be conducted.

Another example of how TRIB3 could control vascular health is through the regulation of an intravascular leukocyte cell adhesion (52). Although our study did not assess leukostasis in the retinas, we did find that similar to patients with diabetes with microalbuminuria and DR (53), *Icam1*, a cell surface glycoprotein expressing on endothelial cells and leukocytes, was significantly upregulated in C57BL/6 mouse diabetic retinas. TRIB3 ablation led to a dramatic reduction of *Icam1* expression. In addition to *Icam1*, we found that TRIB3 controlled the endothelial cell death in diabetic retina and that ablation of TRIB3 significantly preserved the formation of acellular capillaries and subsequent pericyte loss. These data provide evidence that TRIB3 plays a substantial role in endothelial cell homeostasis in DR.

Inflammation is one of the major factors induced during diabetes and leads to macular edema, ischemia, and NV (54). In TRIB3 KO diabetic retinas, the proinflammatory gene expression profile was altered. Moreover, the increase in retinal microglia and VEGF cytokine production was TRIB3 mediated. TRIB3 could directly or indirectly affect expression of NF-κB and other cytokines, thus modifying early inflammatory response to hyperglycemia. In support of this hypothesis, TRIB3 ablation

Additionally, HIF1α mediates VEGF expression, which compromises vascular cell integrity and triggers angiogenesis. EGFR is upregulated as a result of TRIB3 upregulation as well. This protein reportedly induces VEGF and cytokines, leading to vascular dysfunction. TRIB3 promotes expression of GFAP and reactivation of gliosis in hypoxic retinas. Red and purple arrows indicate upregulation, and blue arrows indicate downregulation signaling validated in our study. Solid lines represent data of the current study. Dashed lines denote the regulation proposed in the literature. Data are mean ± SEM. *$P < 0.05$, **$P < 0.01$. a.u., arbitrary units; ER, endoplasmic reticulum.

prevented both neuronal and vascular dysfunction, which serve as hallmarks of DR in humans. Therefore, it is of particular importance that TRIB3 controls RGC death. In hyperglycemic TRIB3 KO mouse retinas, RGC preservation correlated with a significant improvement of the recorded PhNR amplitudes, which are known to be diminished in patients with diabetes (55). Moreover, in concordance with these results, we revealed that in hypoxic retinas, TRIB3 controls retinal integrity too. This latest observation is also supported by the fact that Müller cells overexpressing TRIB3 manifested reduced cell viability.

The limitations of the current study are that we did not access a cell-specific role of TRIB3 in diabetic retinas due to unviability of the mouse model or in primary retinal culture of ganglion, photoreceptor, and endothelial cells. Therefore, future experiments should identify sources of TRIB3-induced cellular damage, "signaling" neurovascular degeneration in diabetic retinas. Nevertheless, regardless of the sources, we found that hypoxic TRIB3 KO retina manifested less gliotic activity of Müller cells as determined by colocalization of vimentin and GFAP. TRIB3-mediated control of GFAP in vivo was confirmed in cultured Müller cells, indicating that TRIB3-mediated GFAP upregulation is independent of HIF1α protein regulation. This finding pinpoints TRIB3 as a novel potential regulator of GFAP biogenesis during diabetes.

Overall, our study indicates that TRIB3 mediates the expression of major sets of hypoxia-induced genes, including HIF1α, EGFR, VEGF, GLUT1, and GFAP—effects that were observed both in vitro and in vivo. Our data align with previous studies conducted in human cancer cells in which TRIB3 was proposed as a molecular regulator of angiogenesis mediated via HIF1α and VEGF upregulation (56). In addition to angiogenesis, our investigation indicated that TRIB3 is a master regulator of early metabolic and inflammatory events in diabetic retinas, which affect the overall development and progression of disease to proliferative stages. Given the limitations and side effects of current treatments for DR and the continuing efforts to understand its complex molecular mechanisms, our findings revealed that TRIB3 is a major game player of diabetic ocular pathophysiology and a novel therapeutic target, the potential of which should be further evaluated in the clinic.

Funding. This work was supported by National Eye Institute grants R01-EY-027763 and R21-EY-031103. The authors also acknowledge support of National Institutes of Health grant P30-DK-079626 to the leukocytosis UAB Diabetes Research Center and Bio-Analytical Redox Biology core facility and National Institute of Diabetes and Digestive and Kidney Diseases grant DK-056336 to the Nutrition Obesity Research Center, UAB Center for Exercise Medicine, UAB Comprehensive Diabetes Center, Center for Free Radical Biology, and UAB Comprehensive Neuroscience Center.

Duality of Interest. No potential conflicts of interest relevant to this article were reported.

Author Contributions. P.M.P., I.V.S., and M.S.G. designed, performed, and analyzed the experiments. P.M.P. and M.S.G. wrote the manuscript. Y.A.-A. helped with the quantitative analysis of retinal cells and analysis of the retinal images. S.L.C. helped with the OIR mouse model and the preparation of retinal flat mounts. T.S. and S.A. developed the mouse model used in the study. O.G. helped with the images and prepared the figures. M.E.B. provided human diabetic retinas. M.E.B., W.T.G., M.A., and M.B.G. helped with the analysis of experimental results. M.T.P. helped to analyze the results of the PhNR recording in diabetic retinas. All authors reviewed and/or edited the manuscript. M.S.G. is the guarantor of this work and, as such, had full access to all the data in the study and takes responsibility for the integrity of the data and the accuracy of the data analysis.

References

1. Stitt AW, Curtis TM, Chen M, et al. The progress in understanding and treatment of diabetic retinopathy. Prog Retin Eye Res 2016;51:156–186

2. Ord T, Ord T. Mammalian pseudokinase TRIB3 in normal physiology and disease: charting the progress in old and new avenues. Curr Protein Pept Sci 2017;18:819–842

3. Oskolkova OV, Afonyushkin T, Leitner A, et al. ATF4-dependent transcription is a key mechanism in VEGF up-regulation by oxidized phospholipids: critical role of oxidized sn-2 residues in activation of unfolded protein response. Blood 2008;112:330–339

4. Fang N, Zhang W, Xu S, et al. TRIB3 alters endoplasmic reticulum stress-induced β-cell apoptosis via the NF-κB pathway. Metabolism 2014;63:822–830

5. Cheng W, Mi L, Tang J, Yu W. Expression of TRB3 promotes epithelial-mesenchymal transition of MLE-12 murine alveolar type II epithelial cells through the TGF-β1/Smad3 signaling pathway. Mol Med Rep 2019;19:2869–2875

6. Steverson D Jr, Tian L, Fu Y, Zhang W, Ma E, Garvey WT. Tribbles homolog 3 promotes foam cell formation associated with decreased proinflammatory cytokine production in macrophages: evidence for reciprocal regulation of cholesterol uptake and inflammation. Metab Syndr Relat Disord 2016;14:7–15

7. Shang YY, Wang ZH, Zhang LP, et al. TRB3, upregulated by ox-LDL, mediates human monocyte-derived macrophage apoptosis. FEBS J 2009;276:2752–2761

8. Gong HP, Wang ZH, Jiang H, et al. TRIB3 functional Q84R polymorphism is a risk factor for metabolic syndrome and carotid atherosclerosis. Diabetes Care 2009;32:1311–1313

9. Prudente S, Hribal ML, Flex E, et al. The functional Q84R polymorphism of mammalian Tribbles homolog TRB3 is associated with insulin resistance and related cardiovascular risk in Caucasians from Italy. Diabetes 2005;54:2807–2811

10. Andreozzi F, Formoso G, Prudente S, et al. TRIB3 R84 variant is associated with impaired insulin-mediated nitric oxide production in human endothelial cells. Arterioscler Thromb Vasc Biol 2008;28:1355–1360

11. Formoso G, Di Tomo P, Andreozzi F, et al. The TRIB3 R84 variant is associated with increased carotid intima-media thickness in vivo and with enhanced MAPK signalling in human endothelial cells. Cardiovasc Res 2011;89:184–192

12. Liew CW, Bochenski J, Kawamori D, et al. The pseudokinase tribbles homolog 3 interacts with ATF4 to negatively regulate insulin exocytosis in human and mouse beta cells. J Clin Invest 2010;120:2876–2888

13. Mondal D, Mathur A, Chandra PK. Tripping on TRIB3 at the junction of health, metabolic dysfunction and cancer. Biochimie 2016;124:34–52

14. Ishikawa K, Yoshida S, Kobayashi Y, et al. Microarray analysis of gene expression in fibrovascular membranes excised from patients with proliferative diabetic retinopathy. Invest Ophthalmol Vis Sci 2015;56:932–946

15. Satoh T, Kidoya H, Naito H, et al. Critical role of Trib1 in differentiation of tissue-resident M2-like macrophages. Nature 2013;495:524–528
16. Smith LE, Wesolowski E, McLellan A, et al. Oxygen-induced retinopathy in the mouse. Invest Ophthalmol Vis Sci 1994;35:101–111
17. Xiao S, Bucher F, Wu Y, et al. Fully automated, deep learning segmentation of oxygen-induced retinopathy images. JCI Insight 2017;2:e97585
18. Limb GA, Salt TE, Munro PM, Moss SE, Khaw PT. In vitro characterization of a spontaneously immortalized human Müller cell line (MIO-M1). Invest Ophthalmol Vis Sci 2002;43:864–869
19. Reiter CE, Wu X, Sandirasegarane L, et al. Diabetes reduces basal retinal insulin receptor signaling: reversal with systemic and local insulin. Diabetes 2006;55:1148–1156
20. Rajala RV, Wiskur B, Tanito M, Callegan M, Rajala A. Diabetes reduces autophosphorylation of retinal insulin receptor and increases protein-tyrosine phosphatase-1B activity. Invest Ophthalmol Vis Sci 2009;50:1033–1040
21. Zou T, Liu WJ, Li SD, Zhou W, Yang JF, Zou CG. TRB3 mediates homocysteine-induced inhibition of endothelial cell proliferation. J Cell Physiol 2011;226:2782–2789
22. Geng T, Hu W, Broadwater MH, et al. Fatty acids differentially regulate insulin resistance through endoplasm reticulum stress-mediated induction of tribbles homologue 3: a potential link between dietary fat composition and the pathophysiological outcomes of obesity. Diabetologia 2013;56:2078–2087
23. Wang W, Cheng J, Sun A, et al. TRB3 mediates renal tubular cell apoptosis associated with proteinuria. Clin Exp Med 2015;15:167–177
24. Oberkofler H, Pfeifenberger A, Soyal S, et al. Aberrant hepatic TRIB3 gene expression in insulin-resistant obese humans. Diabetologia 2010;53: 1971–1975
25. Liu J, Wu X, Franklin JL, et al. Mammalian Tribbles homolog 3 impairs insulin action in skeletal muscle: role in glucose-induced insulin resistance. Am J Physiol Endocrinol Metab 2010;298:E565–E576
26. Borsting E, Patel SV, Declèves AE, et al. Tribbles homolog 3 attenuates mammalian target of rapamycin complex-2 signaling and inflammation in the diabetic kidney. J Am Soc Nephrol 2014;25:2067–2078
27. Zhong Y, Li J, Chen Y, Wang JJ, Ratan R, Zhang SX. Activation of endoplasmic reticulum stress by hyperglycemia is essential for Müller cell-derived inflammatory cytokine production in diabetes. Diabetes 2012;61:492–504
28. Grenell A, Wang Y, Yam M, et al. Loss of MPC1 reprograms retinal metabolism to impair visual function. Proc Natl Acad Sci U S A 2019;116: 3530–3535
29. Johnston J, Basatvat S, Ilyas Z, Francis S, Kiss-Toth E. Tribbles in inflammation. Biochem Soc Trans 2015;43:1069–1074
30. Sakai Y, Tanaka T, Seki M, et al. Cyclooxygenase-2 plays a critical role in retinal ganglion cell death after transient ischemia: real-time monitoring of RGC survival using Thy-1-EGFP transgenic mice. Neurosci Res 2009;65:319–325
31. Martin PM, Roon P, Van Ells TK, Ganapathy V, Smith SB. Death of retinal neurons in streptozotocin-induced diabetic mice. Invest Ophthalmol Vis Sci 2004;45:3330–3336
32. Fortepiani LA, Le D, Akimov NP, Sohn J-H, Rentería RC: Decreased amplitude of the photopic negative response (PhNR) in the Ins2Akita mouse model of type 1 diabetes mellitus [Abstract]. FASEB J 2019:554.7
33. Chen H, Zhang M, Huang S, Wu D. The photopic negative response of flash ERG in nonproliferative diabetic retinopathy. Doc Ophthalmol 2008;117: 129–135
34. Rutkowski P, May CA. Nutrition and vascular supply of retinal ganglion cells during human development. Front Neurol 2016;7:49
35. Wang X, Wang G, Kunte M, Shinde V, Gorbatyuk M. Modulation of angiogenesis by genetic manipulation of ATF4 in mouse model of oxygen-induced retinopathy [corrected]. Invest Ophthalmol Vis Sci 2013;54:5995–6002
36. Ohoka N, Yoshii S, Hattori T, Onozaki K, Hayashi H. TRB3, a novel ER stress-inducible gene, is induced via ATF4-CHOP pathway and is involved in cell death. EMBO J 2005;24:1243–1255
37. Loewen N, Chen J, Dudley VJ, Sarthy VP, Mathura JR Swarthy. Genomic response of hypoxic Müller cells involves the very low density lipoprotein receptor as part of an angiogenic network. Exp Eye Res 2009;88: 928–937
38. Gu L, Xu H, Zhang C, Yang Q, Zhang L, Zhang J. Time-dependent changes in hypoxia- and gliosis-related factors in experimental diabetic retinopathy. Eye (Lond) 2019;33:600–609
39. Brownlee M. The pathobiology of diabetic complications: a unifying mechanism. Diabetes 2005;54:1615–1625
40. Vadlapatla RK, Vadlapudi AD, Mitra AK. Hypoxia-inducible factor-1 (HIF-1): a potential target for intervention in ocular neovascular diseases. Curr Drug Targets 2013;14:919–935
41. Hong B, Zhou J, Ma K, et al. TRIB3 promotes the proliferation and invasion of renal cell carcinoma cells via activating MAPK signaling pathway. Int J Biol Sci 2019;15:587–597
42. Moulin S, Thomas A, Arnaud C, et al. Cooperation between hypoxia-inducible factor 1α and activating transcription factor 4 in sleep apnea-mediated myocardial injury. Can J Cardiol 2020;36:936–940
43. Galbán S, Gorospe M. Factors interacting with HIF-1alpha mRNA: novel therapeutic targets. Curr Pharm Des 2009;15:3853–3860
44. Schofield CJ, Ratcliffe PJ. Signalling hypoxia by HIF hydroxylases. Biochem Biophys Res Commun 2005;338:617–626
45. Liu J, Zhang W, Chuang GC, et al. Role of TRIB3 in regulation of insulin sensitivity and nutrient metabolism during short-term fasting and nutrient excess. Am J Physiol Endocrinol Metab 2012;303:E908–E916
46. Tang J, Zhu XW, Lust WD, Kern TS. Retina accumulates more glucose than does the embryologically similar cerebral cortex in diabetic rats. Diabetologia 2000;43:1417–1423
47. Ramírez-Pérez G, Sánchez-Chávez G, Salceda R. Mitochondrial bound hexokinase type I in normal and streptozotocin diabetic rat retina. Mitochondrion 2020;52:212–217
48. Van den Enden MK, Nyengaard JR, Ostrow E, Burgan JH, Williamson JR. Elevated glucose levels increase retinal glycolysis and sorbitol pathway metabolism. Implications for diabetic retinopathy. Invest Ophthalmol Vis Sci 1995;36:1675–1685
49. Zhou L, Zhang S, Zhang L, Li F, Sun H, Feng J. MiR-199a-3p inhibits the proliferation, migration, and invasion of endothelial cells and retinal pericytes of diabetic retinopathy rats through regulating FGF7 via EGFR/PI3K/AKT pathway. J Recept Signal Transduct Res 2021;41:19–31
50. Sugimoto M, Cutler A, Shen B, et al. Inhibition of EGF signaling protects the diabetic retina from insulin-induced vascular leakage. Am J Pathol 2013;183:987–995
51. Lee SH, Koo KH, Park JW, et al. HIF-1 is induced via EGFR activation and mediates resistance to anoikis-like cell death under lipid rafts/caveolae-disrupting stress. Carcinogenesis 2009;30:1997–2004
52. Sowers JR. Role of TRIB3 in diabetic and overnutrition-induced atherosclerosis. Diabetes 2012;61:265–266
53. Meleth AD, Agrón E, Chan CC, et al. Serum inflammatory markers in diabetic retinopathy. Invest Ophthalmol Vis Sci 2005;46:4295–4301
54. Bandello F, Lattanzio R, Zucchiatti I, Del Turco C. Pathophysiology and treatment of diabetic retinopathy. Acta Diabetol 2013;50:1–20
55. Kizawa J, Machida S, Kobayashi T, Gotoh Y, Kurosaka D. Changes of oscillatory potentials and photopic negative response in patients with early diabetic retinopathy. Jpn J Ophthalmol 2006;50:367–373
56. Dong S, Xia J, Wang H, et al. Overexpression of TRIB3 promotes angiogenesis in human gastric cancer. Oncol Rep 2016;36:2339–2348